

Regulation of Glucose-Dependent Gene Expression by the RNA Helicase Dbp2 in *Saccharomyces cerevisiae*

Zachary T. Beck,^{*1} Sara C. Cloutier,^{*1} Matthew J. Schipma,[†] Christopher J. Petell,^{*} Wai Kit Ma,^{*} and Elizabeth J. Tran^{*,1,2}

^{*}Department of Biochemistry, Purdue University, West Lafayette, Indiana 47907-2063, [†]Purdue University Center for Cancer Research, Purdue University, West Lafayette, Indiana 47907-2064, and [‡]Next Generation Sequencing Core Facility, Feinberg School of Medicine, Northwestern University, Chicago, Illinois 60611

ABSTRACT Cellular homeostasis requires a fine balance between energy uptake, utilization, and growth. *Dbp2* is a member of the DEAD-box protein family in *Saccharomyces cerevisiae* with characterized ATPase and helicase activity *in vitro*. DEAD-box RNA helicases are a class of enzymes that utilize ATP hydrolysis to remodel RNA and/or RNA–protein (RNP) composition. *Dbp2* has been proposed to utilize its helicase activity *in vivo* to promote RNA–protein complex assembly of both messenger (m)RNAs and long noncoding (lnc)RNAs. Previous work from our laboratory demonstrated that loss of *DBP2* enhances the lncRNA-dependent transcriptional induction of the *GAL* genes by abolishing glucose-dependent repression. Herein, we report that either a carbon source switch or glucose deprivation results in rapid export of *Dbp2* to the cytoplasm. Genome-wide RNA sequencing identified a new class of antisense hexose transporter transcripts that are specifically upregulated upon loss of *DBP2*. Further investigation revealed that both sense and antisense hexose transporter (*HXT*) transcripts are aberrantly expressed in *DBP2*-deficient cells and that this expression pathway can be partially mimicked in wild-type cells by glucose depletion. We also find that *Dbp2* promotes ribosome biogenesis and represses alternative ATP-producing pathways, as loss of *DBP2* alters the transcript levels of ribosome biosynthesis (snRNAs and associated proteins) and respiration gene products. This suggests that *Dbp2* is a key integrator of nutritional status and gene expression programs required for energy homeostasis.

CELL growth and division is intimately coupled to cell mass, with the nutrient availability and ribosome content playing a key role in dictating growth rate (Lempiainen and Shore 2009). This involves phosphorylation cascades such as the TOR (target of rapamycin) and the Ras–cAMP–protein kinase A signaling pathways to transmit information regarding the availability of nutrients to essential processes for cell growth (Powers and Walter 1999; Warner 1999; Lempiainen and Shore 2009; Broach 2012).

Dbp2 is a member of the DEAD-box RNA helicase family in the budding yeast *Saccharomyces cerevisiae*. DEAD-box proteins are RNA-dependent ATPases that utilize ATP hydrolysis

to catalyze structural rearrangements to RNA and RNA–protein (RNP) complexes (Bowers *et al.* 2006; Bhaskaran and Russell 2007; Del Campo *et al.* 2009; Jankowsky 2011; Putnam and Jankowsky 2013b). The metazoan ortholog of *Dbp2*, hDDX5, or p68 has been linked to ribosome biogenesis as well as a variety of gene regulatory processes including transcriptional regulation, alternative splicing, and mRNA export (Wilson *et al.* 2004; Buszczak and Spradling 2006; Caretti *et al.* 2006; Jalal *et al.* 2007; Salzman *et al.* 2007; Camats *et al.* 2008; Clark *et al.* 2008; Fuller-Pace and Moore 2011). Budding yeast *Dbp2* is also required for ribosome biogenesis and numerous processes linked to transcriptional fidelity (Barta and Iggo 1995; Bond *et al.* 2001; Bohnsack *et al.* 2009; Cloutier *et al.* 2012; Cloutier *et al.* 2013; Ma *et al.* 2013).

Biochemical characterization has established that *Dbp2* is a *bona fide* helicase and ATPase *in vitro*, with robust duplex unwinding in line with other DEAD-box proteins (Cloutier *et al.* 2012; Kovalev *et al.* 2012; Ma *et al.* 2013). *Dbp2* associates directly with actively transcribed chromatin, suggestive of a cotranscriptional role (Cloutier *et al.* 2012). Moreover,

Copyright © 2014 by the Genetics Society of America
doi: 10.1534/genetics.114.170019

Manuscript received June 9, 2014; accepted for publication August 20, 2014; published Early Online August 27, 2014.

Supporting information is available online at <http://www.genetics.org/lookup/suppl/doi:10.1534/genetics.114.170019/-/DC1>.

¹These authors contributed equally to this work.

²Corresponding author: Department of Biochemistry, Purdue University, BCHM 305, 175 S. University St., West Lafayette, IN 47907. E-mail: ejtran@purdue.edu

loss of *DBP2* results in decreased association of mRNA-binding proteins and nuclear export factors *Yra1*, *Nab2*, and *Mex67* to mRNA (Ma *et al.* 2013). This has led to the model that *Dbp2* promotes mRNP assembly by modulating nascent RNA structure during transcription.

Recent work from our laboratory connected the RNA helicase *Dbp2* to long noncoding RNA (lncRNA)-dependent gene regulation (Cloutier *et al.* 2013). Although the precise molecular role(s) for the >30,000 eukaryotic lncRNAs identified thus far is not well defined, an emerging theme is that lncRNAs fine tune transcriptional switches in gene expression (Fatica and Bozzoni 2014). The *GAL* cluster genes are part of the galactose metabolic switch that allows budding yeast to rapidly adapt to the availability of galactose as an alternative to glucose as a carbon source (Lohr *et al.* 1995; Sellick *et al.* 2008). This switch involves a number of carbon source sensors, sugar transporters, signaling cascades, and transcriptional effectors to globally alter the metabolic program for energy production (Gancedo 1998; Johnston and Kim 2005; Traven *et al.* 2006; Broach 2012). Interestingly, our work revealed that the *GAL* lncRNAs function in this switch by enhancing the transcriptional response rate to the carbon source switch (Cloutier *et al.* 2013). *Dbp2* antagonizes this role by maintaining glucose-dependent repression of the *GAL* genes, with loss of *DBP2* enhancing transcriptional induction in an lncRNA-dependent manner (Cloutier *et al.* 2013). This suggests that *Dbp2* may be fundamentally integrated into gene regulatory programs that are responsive to nutritional status of the cell.

Herein, we show that *Dbp2* plays a global role in glucose-dependent repression. Our results suggest that this RNA helicase is both regulated by carbon source availability and controls expression of energy-producing and -consuming gene expression networks. We also document a class of lncRNAs that are antisense to hexose transporter genes and show that the levels of these lncRNAs are dependent on *Dbp2*. These results are intriguing because glucose-dependent repression is primarily maintained by transcription factors whose activity is controlled by cellular signaling cascades. Our work now establishes a role for an RNA helicase in this process, indicating that gene expression networks may also be regulated by modulation of RNA structure.

Materials and Methods

Yeast strains

The strains used in this study include: *DBP2-GFP*, MATa *DBP2-GFP:HIS3 his3Δ1 leu2Δ0 met15Δ0 ura3Δ0*; wild type, MATa *his3Δ1 leu2Δ0 met15Δ0 ura3Δ0 dbp2Δ* (BTY115), MATa *dbp2::KanMx6 his3Δ1 leu2Δ0 met15Δ0 ura3Δ0*; *msn5Δ DBP2-GFP* MATa *msn5::KanMx6 DBP2-GFP:HIS3 his3Δ1 leu2Δ0 met15Δ0 ura3Δ0*; *snf1Δ DBP2-GFP* MATa *snf1::KanMx6 DBP2-GFP:HIS3 his3Δ1 leu2Δ0 met15Δ0 ura3Δ0*; *hog1Δ DBP2-GFP*, MATa *hog1::KanMx6 DBP2-GFP:HIS3 his3Δ1 leu2Δ0 met15Δ0 ura3Δ0*; *DBP2-FLAG* MATa *his3Δ1 leu2Δ0*

Table 1 Oligonucleotides for qPCR

| | |
|--------------------------|-------------------------|
| ACT1 forward | TGGATTCCGGTGATGGTGTT |
| ACT1 reverse* | TCAAAATGGCGTGAGGTAGAGA |
| HXT1 forward** | GAATTGGAATCTGGTCGTTT |
| HXT1 reverse* | TAGACACCTTTTCCGGTGTT |
| HXT4 forward** | CCGCCTACGTTACAGTTTCC |
| HXT4 reverse* | ACAAAACCACCGAAAGCAAC |
| HXT5 sense forward | GCCGGTTACAACGATAAATTTGG |
| HXT5 sense reverse* | GGCCTTCATGGGAAATGTAAC |
| HXT5 antisense forward** | TTTCTGCCCACTTCTCTTACAA |
| HXT5 antisense reverse | CCGTCCTCACTGTTTTATTACAA |
| HXT8 forward** | TTCCATTAAGGGTGAGATCCAA |
| HXT8 reverse | CGATTAGGAACCCCAATAA |

Oligonucleotides for quantitative PCR after reverse transcription (RT-qPCR). Oligonucleotides for RT-qPCR are listed as forward and reverse pairs for each transcript tested. Primers used for strand-specific cDNA preparation are indicated with one asterisk corresponding to a primer for sense and two asterisks for antisense. QPCR was conducted with both forward and reverse primer pairs.

met15Δ0 ura3Δ0 DBP2-3xFLAG:KanMx6. All strains are in the BY4741 strain background. *DBP2-GFP* is available from Invitrogen whereas wild type is available from Open Biosystems. The *dbp2Δ* strain was constructed by PCR-mediated gene replacement as previously described (Cloutier *et al.* 2012). The *msn5Δ DBP2-GFP* and *snf1Δ DBP2-GFP* strains were constructed by PCR-mediated integration of a GFP tag into *DBP2* genomic locus in the the *msn5Δ*, *snf1Δ*, and *hog1Δ* strains available from Open Biosystems.

Preparation and purification of anti-Dbp2

Polyclonal rabbit anti-Dbp2 antibodies were generated by Cocalico Biologicals, Inc., using full-length, recombinant purified *Dbp2* expressed in bacteria (Cloutier *et al.* 2012). Resulting immunosera was dialyzed against PBS and subjected to affinity purification using *Dbp2*-conjugated CNBr-sepharose according to manufacturer's instructions (Sigma). The eluted, purified anti-Dbp2 antibody was stored at 4° in the presence of 0.05% sodium azide. Western blotting was conducted with a 1:5000 dilution of anti-Dbp2.

Fluorescent cell microscopy

Cells were initially grown to an OD_{600 nm} of 0.1 at 30° in YP + 2% Glucose (YPD). Cells were washed twice with YP + 0% Glucose (YP) and then resuspended in YP + different concentrations of glucose as indicated. Cells were harvested by centrifugation at the indicated time points and were visualized using an Olympus BX-51 fluorescent microscope. For translational shut-off assays, cells grown in YPD were shifted to YP and then back to YPD with or without 300 μg/ml cycloheximide for 30 min before visualization. Where indicated, 10 μg/ml rapamycin was included. Images were captured with a Hamamatsu Orca R2 camera and MetaMorph software (Molecular Devices, Sunnyvale, CA).

Quantitative Western blotting

Protein stability was assayed following addition of cycloheximide to the media as above, but with 20 μg/ml of cycloheximide. Yeast cell lysates were prepared as described previously (Cloutier *et al.* 2013). *Dbp2*, *Upf1*, and *Pgk1* were detected using

Table 2 Oligonucleotides for Chromatin Immunoprecipitation (ChIP)

| Name | Forward primer | Reverse primer | Probe |
|----------------|-----------------------|--------------------------|----------------------------|
| HXT1 antisense | TTCCAGGCTGTCGGTTAAG | AGCACCCCACATCAAACAG | CCAAAACGGTCAACGGTGTAC |
| HXT1 sense | GGCCATGAATACTCCAGAAGG | CACCGAAAGCAACCATAACAC | AGTGAAGTCAAGTGAACCCCG |
| HXT4 sense | GTTGGTGTACAAGATTGTGGC | CAGGTAGTGGCAAAACAGAATAAG | AACGGGTCTTCTAAGGGTGTGG |
| HXT5 antisense | TACTCGAGGTTTCAACAGGG | AGGTAGCGGAGTTTCAGTTC | AATCAAGAGCCCCGTCTTTTACCGT |
| HXT5 sense | CGGAACCTGAAAACGCTCATC | TGAGACGGGTTTAGCTTGTG | CCTTGAAGGGTCTGCTACTGTGA |
| HXT8 antisense | TCTGTTGATAAGTTGGGCCG | GTAATAACCATGCACGCCG | TCTTTTACTTGGAGCAGCCACCATGA |
| HXT8 sense | TTAGTGTCTTGCCCCGATG | CGAAAGTCACCATCAATTGCC | ACTGCGCCAAAGCATATCAGAGGT |

Oligonucleotides for ChIP are Primetime qPCR assays (IDT) and are listed as forward and reverse primers and probe for each gene tested.

rabbit anti-Dbp2 (this study), rabbit anti-Upf1 (Bond *et al.* 2001), or mouse anti-Pgk1 (459250, Invitrogen) respectively. Proteins were visualized using Luminata Crescendo Western HRP Substrate (Millipore) according to manufacturer's instructions. Bands were quantified using ImageQuant TL software (GE Life Sciences).

RNA sequencing sample preparation

Wild-type and *dbp2Δ* cells were grown in YPD at 30° to an OD_{600 nm} of 0.4 before being harvested by centrifugation, flash frozen in liquid nitrogen, and stored at -80°. Total RNA isolation was performed using a standard acid phenol:chloroform purification as previously described (Cloutier *et al.* 2012). DNase treatment was performed using 1 U TurboDNase (Life Technologies) per 10 μg of RNA for 30 min at 37°. RNA was analyzed with a DU-730 Beckman-Coulter spectrophotometer. RNA purity was considered suitable for qPCR if the A_{260/280} was ~2.0 and the yield was ~80% after DNase treatment.

Ribosomal RNA depletion was performed prior to library generation (Ribominus Eukaryote kit, Life Technologies). A strand-specific RNA sequencing library was generated using paired-end reads and SOLiD sequencing on the 5500 XL platform (Life Technologies) by the Northwestern University Genomics Core Facility. Forward sequences were generated using the F3 tag and were 75 bp in length; reverse sequences were generated with the F5 tag and were 35 bp in length.

RNA sequencing data analysis

RNA sequencing generated ~60 million and 40 million mappable reads in wild type and *dbp2Δ*, respectively, per replicate. Raw data quality was evaluated by FastQC software with Illumina 1.9 encoding. Reads were aligned by position and orientation to the reference *S. cerevisiae* genome sacCer3 (<http://www.genome.ucsc.edu>) using LifeScope v. 2.5.1. Gene expression (in RPKM), statistical analysis, and fold change between strains were determined using Cufflinks 2.0 software. Those genes with a statistically significant increase in transcripts in *dbp2Δ* were analyzed for GO-term enrichment for similar processes using FuncAssociate 2.0 (<http://llama.mshri.on.ca/funcassociate/>) (Berriz *et al.* 2009). RNA sequencing data are deposited in the NCBI GEO database no. GSE58097.

Strand-specific RT-qPCR

Primers for RT-qPCR were designed using Primer Express 3.0 software. Strand-specific reverse transcription was performed

using the Quantitect reverse transcription kit (Qiagen) with the following modifications: A total amount of 2 μg of RNA was prepared for a 20 μl reaction. Primers specific to one strand of the target gene and the sense strand of a reference gene, *ACT1*, were added to a final concentration of 5 μM. Actinomycin D was included in the reverse transcription reaction to a final concentration of 6 ng/μl to prevent second-strand synthesis. Following heat inactivation, unincorporated primers were removed using the QiaQuick PCR Purification Kit (Qiagen) according to the manufacturer's instructions. Quantitative PCR was performed as previously described (Cloutier *et al.* 2012). Fold changes were calculated using the Pfaffl method (Pfaffl 2001), with results reported as the mean ±SE of three biological replicates with three technical repeats. See Table 1 for a listing of primers used for strand-specific reverse transcription.

Chromatin immunoprecipitation

Chromatin immunoprecipitation (ChIP) was performed as described previously (Cloutier *et al.* 2012). Primer-probe sets were designed to amplify DNA corresponding to the genomic regions to the 5' ends of the sense and antisense transcripts of *HXT1*, *HXT5*, and *HXT8* and the region corresponding to the sense transcript of *HXT4*. Results represent three biological replicates with three technical replicates shown as the mean percentage signal above input and SEM. Primetime assay primer-probe sets (IDT) are listed in Table 2.

Results

The cellular localization of Dbp2 is responsive to extracellular glucose

Many glucose-dependent repressors are regulated at the level of cellular localization, protein stability, and/or synthesis in response to nutrient availability (Gancedo 1998). Moreover, recent global analyses of mRNP complexes in budding yeast revealed that the subcellular distribution of a large proportion of RNA-binding proteins is dictated by environmental growth conditions (Mitchell *et al.* 2013). To determine if *Dbp2* is regulated similarly, we first examined the localization of a C-terminally GFP-tagged *Dbp2* in *S. cerevisiae* during the shift from glucose to galactose (Figure 1A). Briefly, strains expressing a genomically encoded *DBP2-GFP* were grown to early log phase (OD_{600 nm} of 0.1) in standard, rich media

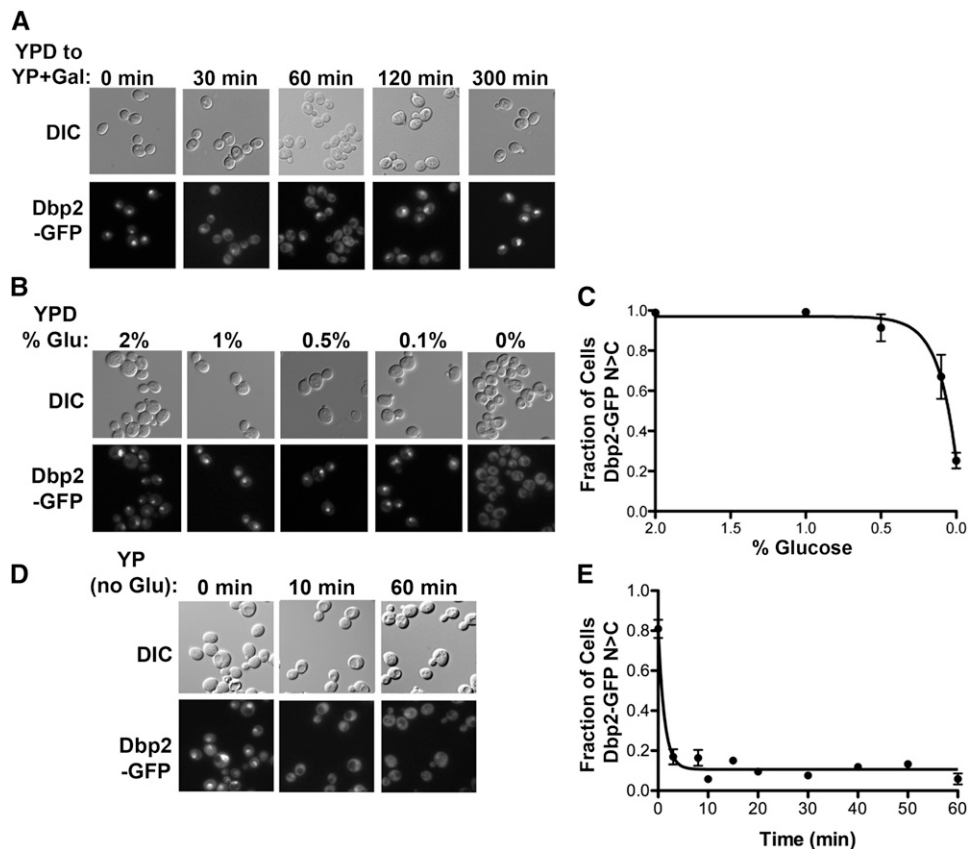


Figure 1 Dbp2 is redistributed to the cytosol upon glucose deprivation. (A) The nuclear Dbp2-GFP signal is rapidly lost during a shift from glucose to galactose media. Dbp2-GFP cells were grown in the presence of 2% glucose (YPD) and shifted to media with 2% galactose (YP + Gal). Fluorescent images were collected by microscopy at the indicated time points following the shift. (B) Nuclear Dbp2-GFP signal decreases with lower glucose concentrations. Yeast cells expressing a C-terminally GFP-tagged Dbp2 encoded within the endogenous *DBP2* locus were grown to early log phase (0.1 OD at 600 nm) at 30° in rich media + 2% glucose (YPD) and then shifted to media with the indicated glucose concentrations for 30 min. The localization of Dbp2-GFP was determined by fluorescent microscopy (bottom) with corresponding DIC images (top). All images were collected with the same exposure time and are scaled equivalently. (C) Graphical representation of glucose-dependent nuclear localization of Dbp2. Dbp2-GFP localization was determined as above over a range of glucose concentrations. The fraction of cells with a predominantly nuclear Dbp2-GFP signal is reported for each glucose concentration tested. Graphical points represent the average of three biological replicates with

>100 cells per replicate counted and scored. Error bars represent the SEM. (D) Dbp2 is rapidly lost from the nucleus after glucose removal. Fluorescence microscopy images of Dbp2-GFP localization at the indicated time points following depletion of glucose (YP) are shown. DIC and fluorescence microscopy images were collected as above following growth of Dbp2-GFP-expressing yeast cells in rich media with glucose to early log phase and subsequent removal by centrifugation and resuspension in media lacking glucose. (E) Graphical analysis of the rate of nuclear Dbp2-GFP loss following removal of glucose. The time for Dbp2-GFP relocalization following glucose depletion was determined by growing Dbp2-GFP-expressing cells in YP+2% glucose as above, rapidly shifting the cells to YP lacking glucose and collecting images by fluorescence microscopy at the indicated time points before (0 min) and immediately following glucose depletion. The fraction of cells with nuclear signal was determined as in C.

(YP) plus 2% glucose and then shifted to rich media plus 2% galactose. The cellular localization of Dbp2-GFP was determined by epifluorescent microscopy of samples before (0 min) or at different time points following readdition of galactose.

Consistent with previous studies, Dbp2-GFP displayed a predominantly nuclear localization when cells were grown in the presence of glucose (Figure 1A, 0 min, Cloutier *et al.* 2012). However, Dbp2-GFP redistributed to the cytosol after the carbon source shift (Figure 1A, 30 and 60 min). Interestingly, the nuclear localization was restored by 300 min, suggesting that the cellular redistribution of Dbp2-GFP is due to the removal of glucose, not the presence of galactose. To test this, we asked if reduction of glucose concentrations in the media would also render Dbp2 cytoplasmic. Interestingly, Dbp2 exhibited cytosolic localization only upon full glucose deprivation (0%), whereas Dbp2 is largely nuclear at all tested concentrations (Figure 1, B and C). Next, we asked how quickly cytoplasmic redistribution occurs by conducting a microscopy time course immediately prior to and following removal of glucose from the media (Figure 1, D and E). This revealed that Dbp2-GFP is redistributed to the cytosol within 2 min following glucose removal, indicating a rapid alteration

of cellular localization (Figure 1E). Moreover, the cytosolic localization persisted over a 1-hr time frame (Figure 1, D and E), indicating that the redistribution is both rapid and stable.

The change in Dbp2 localization is due to nuclear transport not protein turnover

The apparent cellular redistribution of Dbp2 could be due to active nuclear export and/or protein turnover. To test this, we measured Dbp2 protein stability by quantitative Western blotting over time following addition of the translational inhibitor cycloheximide. Dbp2 levels were then plotted with respect to the loading control Pgk1 (Figure 2, A and B). Consistent with prior data stating that Dbp2 is exceptionally stable with an estimated half-life of ~250 min (Laxman *et al.* 2010), we did not observe an appreciable decrease within the 1-hr time frame of our analysis. This was not due to an incomplete translational block, as the levels of another RNA helicase, Upf1, was degraded with a half-life within the range of other studies (Figure 2A, red; Ruiz-Echevarria *et al.* 1998). Furthermore, the stability of Dbp2 did not change upon removal of glucose within 1 hr (Figure 2B). This suggests that protein turnover is not a major mechanism for the observed relocalization.

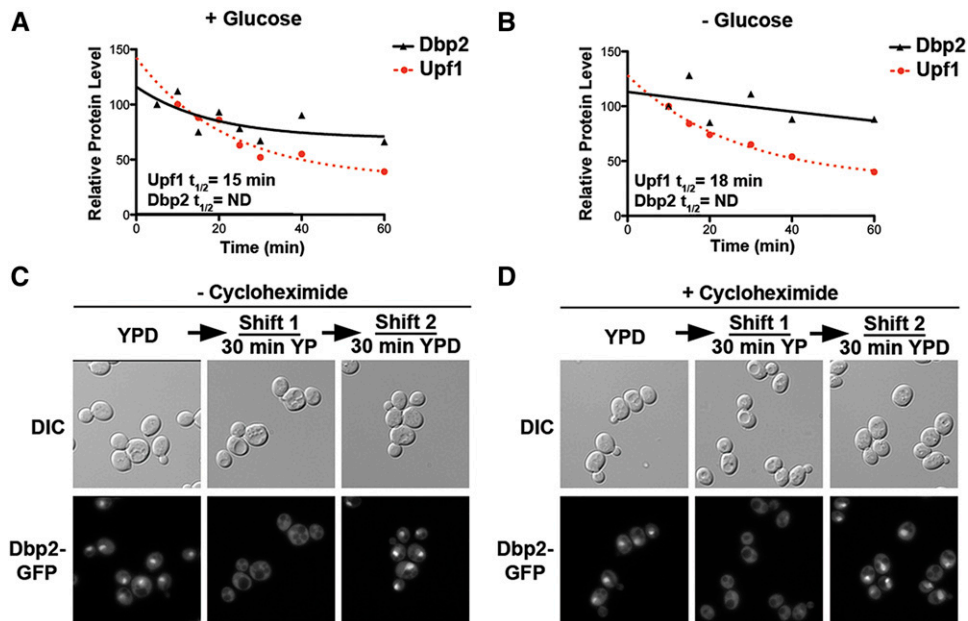


Figure 2 The change in cellular localization of Dbp2 is due to nuclear transport, not protein turnover. (A and B) Dbp2 protein exhibits similar stability irrespective of the presence of glucose in the media. The stability of Dbp2 protein in the presence of glucose (A) or following glucose deprivation (B) by adding cycloheximide, as previously described to prevent new protein synthesis (Castoralova *et al.* 2012). Samples were removed at 5-, 10-, 20-, 30-, 40-, and 60-min increments and subjected to Western blotting with rabbit polyclonal anti-Dbp2. Dbp2 levels were quantified with respect to Pgk1 and are presented graphically. Upf1, another RNA helicase, has a reported half-life of ~16 min (Ruiz-Echevarria *et al.* 1998) and is included as a control for efficient translational shutoff. Dbp2 half-lives could not be determined for either growth conditions because they do not decrease substantially within a 1-hr time frame. (C) Read-

dition of glucose to glucose-deprived cells restores nuclear Dbp2 signal. Dbp2-GFP-expressing cells were subjected to a 30-min glucose deprivation, to ensure complete cytosolic redistribution, and were then resuspended in fresh media with saturating glucose (2%). Dbp2-GFP was visualized before glucose removal (0 min), following deprivation, and after 30 min incubation with fresh, glucose-containing media. Dbp2 localization was visualized by fluorescent microscopy as above. Note that Dbp2-GFP-expressing strains show reduced signal in the absence of glucose (middle). However, this is not due to a change in Dbp2 protein levels (see Figure 2A). (D) New protein synthesis is not necessary for restoration of nuclear signal upon glucose readdition. Dbp2-GFP localization was determined as in C, but in the presence of cycloheximide to block translation.

We then asked if nuclear signal could be restored upon readdition of glucose (Figure 2C). To this end, we subjected cells to a 30-min glucose depletion followed by a 30-min incubation in the presence of glucose (2%). Fluorescent microscopy revealed that the predominantly nuclear localization of Dbp2 was fully restored by adding back glucose (Figure 2C). Moreover, the addition of cycloheximide had no effect on this nuclear accumulation (Figure 2D). This is similar to the regulated localization of the glucose-dependent repressor Mig1 (De Vit *et al.* 1997) and suggests that relocalization of Dbp2 upon glucose deprivation occurs through regulated nucleocytoplasmic transport.

Transport of Dbp2 is not dependent on the Snf1/Msn5, Hog1, or TOR signaling pathways

Upon reduction in extracellular glucose, Mig1 is exported to the cytoplasm through the activity of Snf1, the budding yeast ortholog of the human AMP-activated protein kinase AMPK (Woods *et al.* 1994; De Vit *et al.* 1997; Hardie *et al.* 2012), and the export receptor Msn5 (DeVit and Johnston 1999). To determine if the Snf1 signaling pathway is involved in Dbp2 relocalization, we constructed *DBP2-GFP snf1Δ* cells through standard yeast genetic methods and conducted cellular microscopy following glucose deprivation as above. In contrast to Mig1, Dbp2-GFP was still localized to the cytoplasm following glucose removal in *SNF1*-deficient strains (Figure 3A, left and middle). Moreover, loss of *MSN5* had no effect on relocalization of Dbp2-GFP to the cytoplasm (Figure 3A, right). This suggests that export of Dbp2 upon glucose deprivation is not dependent on the Snf1 signaling pathway. We also

observed efficient cytoplasmic relocalization of Dbp2-GFP in the absence of *HOG1*, a mitogen-activated protein kinase involved in osmolaric stress responses that has recently been linked to glucose deprivation (Westfall *et al.* 2004; Piao *et al.* 2012; Figure 3B).

We then asked if the glucose-dependent cellular localization of Dbp2 is an effect of inhibited reimport rather than stimulated export. The TOR signaling pathway promotes anabolic processes that promote cell growth (Wullschlegler *et al.* 2006). To determine if the localization of Dbp2-GFP requires TOR signaling, we performed cellular microscopy following glucose removal and readdition in the presence of the TOR inhibitor, rapamycin. The translational inhibitor, cycloheximide, was also included to ensure that perceived changes in cellular localization were not due to new protein synthesis. Dbp2-GFP, however, was efficiently reimported upon addition of glucose regardless of the presence of rapamycin (Figure 3C, compare to Figure 2, C and D). Thus, the cytoplasmic relocalization of Dbp2 is not dependent upon Snf1 or Hog1 signaling and neither import nor export of Dbp2 requires TOR. This suggests that the cellular localization of Dbp2 is dependent on another, as-of-yet unidentified signaling pathway or that multiple pathways dictate the glucose-dependent localization of Dbp2 (see Discussion).

DBP2 facilitates glucose-dependent regulation of multiple gene expression networks

Dbp2 is a *bona fide* RNA helicase that associates directly with transcribed chromatin (Cloutier *et al.* 2012; Ma *et al.* 2013). However, our data above suggest that this enzyme

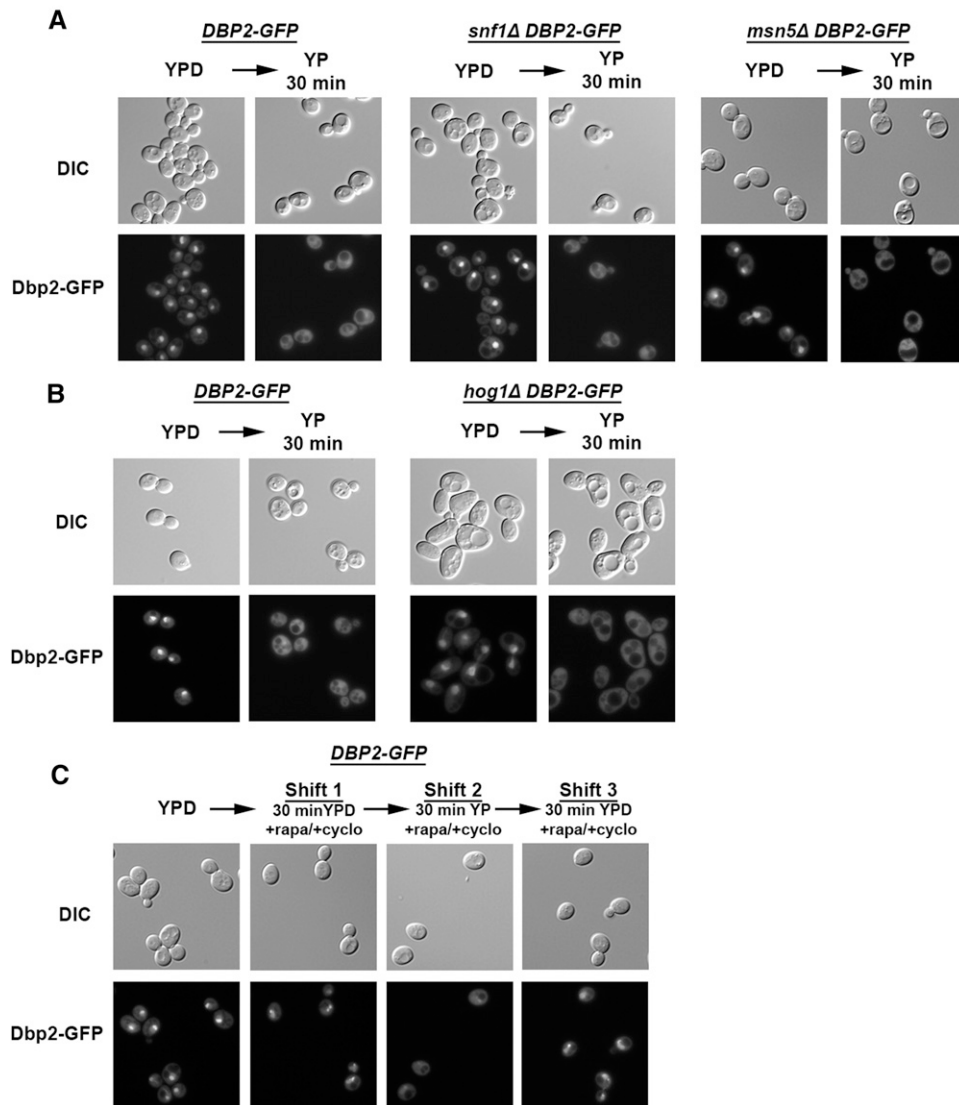


Figure 3 The cellular redistribution of Dbp2 upon glucose deprivation does not depend on the Snf1 pathway, Hog1 pathway, or TOR signaling. (A) Dbp2-GFP signal relocation is not dependent on the Snf1 kinase pathway. Wild-type, *snf1Δ*, and *msn5Δ* cells harboring genomically encoded *DBP2-GFP* constructs were visualized for Dbp2 localization in the presence of glucose (YPD) or after a 30-min deprivation (YP 30 min). Dbp2-GFP was visualized by epifluorescent microscopy and images are representative of three biological replicates. (B) Dbp2-GFP signal is not redistributed to the cytoplasm via the HOG1 osmolaric stress response pathway. Dbp2-GFP localization in wild-type and *hog1Δ* cells was visualized in both the presence of glucose (YPD) and following a 30-min glucose deprivation (YP 30 min) as above. (C) Glucose-dependent localization of Dbp2-GFP is not dependent on the TOR pathway. Dbp2-GFP cells were grown in the presence of glucose (YPD) and then shifted to YPD supplemented with rapamycin and cycloheximide to inhibit the TOR pathway and cycloheximide to inhibit *de novo* protein synthesis (Shift 1). Cells were then subjected to a 30-min glucose deprivation (YP 30 min) in the presence of rapamycin and cycloheximide (Shift 2). After glucose deprivation, cells were given access to glucose (YPD) supplemented with rapamycin and cycloheximide (Shift 3). Fluorescent images were collected as above.

may function more like a carbon-source-regulated transcription factor. Consistent with this, *Dbp2* is required for glucose-dependent repression of the *GAL* cluster genes through modulation of associated long noncoding RNAs (Cloutier *et al.* 2013). To determine if *Dbp2* plays a more widespread role in nutrient-dependent gene expression, we conducted RNA sequencing of wild-type and *dbp2Δ* cells using SOLiD NextGen technology to reveal the entire complement of transcripts whose levels depend on *DBP2*. This resulted in ~50 million mappable reads per strain per replicate, which were then subjected to bioinformatics analysis and alignment to the *S. cerevisiae* genome (Supporting Information, Table S1). Transcripts were separated by sense vs. antisense orientation with respect to the protein-coding gene and fold change from wild type was determined using Cufflinks 2.0 (Table S2 and Table S3, respectively).

RNA seq identified ~3000 coding and noncoding (nonribosomal) transcripts that are either over- or underrepresented in *DBP2*-deficient cells as compared to wild type. To determine if these differentially expressed transcripts fall into common

functional categories, we then conducted GO term analysis using FuncAssociate 2.0 (Berriz *et al.* 2009). Consistent with the link between *Dbp2* and carbon source availability, GO classification revealed a robust overaccumulation of transcripts encoding mitochondrial respiration components (Table 3). *S. cerevisiae* preferentially utilize aerobic fermentation over oxidative respiration for energy production until fermentable carbon sources, such as glucose, become limiting (Broach 2012). These genes are typically repressed in wild-type cells to promote fermentation over oxidation in the presence of glucose. Conversely, transcripts encoding ribosome biogenesis factors, whose expression is activated by glucose, were underrepresented in *dbp2Δ* cells (Table 4). Ribosome biogenesis is also dictated by nutrient availability, balancing energy production with consumption (Warner 1999; Broach 2012). Taken together, this indicates that *DBP2* links nutrient availability to the energy status of the cell.

Unexpectedly, our analysis also revealed accumulation of antisense transcripts overlapping hexose transporter genes (Table 5). Hexose transport constitutes an essential and

Table 3 Upregulated Sense Transcripts (895)

| <i>N</i> | LOD | <i>P</i> | <i>P</i> _{adj} | attrib ID | attrib name |
|----------|-------------|----------|-------------------------|------------|--|
| 9 | 1.278165325 | 4.12E-06 | 0.001 | GO:0006122 | Mitochondrial electron transport, ubiquinol to cytochrome c |
| 8 | 1.229371024 | 2.03E-05 | 0.012 | GO:0005750 | Mitochondrial respiratory chain complex III |
| 8 | 1.229371024 | 2.03E-05 | 0.012 | GO:0045275 | Respiratory chain complex III |
| 8 | 1.083144865 | 6.35E-05 | 0.043 | GO:0005991 | Trehalose metabolic process |
| 10 | 1.066652419 | 9.00E-06 | 0.006 | GO:0005199 | Structural constituent of cell wall |
| 12 | 1.056106801 | 1.29E-06 | <0.001 | GO:0070469 | Respiratory chain |
| 20 | 0.953976428 | 3.53E-09 | <0.001 | GO:0022904 | Respiratory electron transport chain |
| 24 | 0.580122409 | 3.65E-06 | 0.001 | GO:0015078 | Hydrogen ion transmembrane transporter activity |
| 25 | 0.571861779 | 2.95E-06 | <0.001 | GO:0022900 | Electron transport chain |
| 24 | 0.483759772 | 5.38E-05 | 0.033 | GO:0015077 | Monovalent inorganic cation transmembrane transporter activity |
| 49 | 0.4055929 | 6.90E-07 | <0.001 | GO:0001071 | Nucleic acid binding transcription factor activity |
| 49 | 0.4055929 | 6.90E-07 | <0.001 | GO:0003700 | Sequence-specific DNA binding transcription factor activity |
| 50 | 0.30780812 | 6.48E-05 | 0.043 | GO:0006091 | Generation of precursor metabolites and energy |
| 60 | 0.27626111 | 7.13E-05 | 0.046 | GO:0043565 | Sequence-specific DNA binding |

Transcripts encoding respiration and energy production factors are upregulated in *dbp2Δ* cells. RNA sequencing was conducted for wild-type and *dbp2Δ* cells grown at 30° in YP + 2%D using a SOLiD platform and pairwise analysis. Sense and antisense reads were differentiated using Cufflinks 2.0. Resulting transcripts were analyzed as separate data sets depending on over- or underrepresentation and sense vs. antisense orientation with respect to the gene. Genes with sense transcripts that were overrepresented in *dbp2Δ* cells as compared to wild type were selected from the RNA sequencing data set. Gene ontology (GO) terms for functional processes were determined using FuncAssociate 2.0 (<http://lama.mshri.on.ca/funcassociate/>) (Berriz *et al.* 2009). The columns are as follows: *N*, no. of entries in the category; LOD, Log₁₀ of the odds ratio; *P*, one-sided *P*-value of the association of attribute and query; *P*_{adj}, adjusted *P*-value as a fraction of 1000 null-hypothesis simulations; attrib ID, GO term identification number for attribution category; attrib name, category name for functional processes. RNA sequencing data are deposited in GEO, no. GSE58097.

rate-limiting step in sugar catabolism, with hexose transporters providing the sole portal for cellular import of fructose, mannose, and glucose (Johnston and Kim 2005; Horak 2013). Although the function of the hexose transporter (*HXT*) antisense transcripts is not known, this strong GO term enrichment suggests that *Dbp2* may regulate expression of the *HXT* genes via lncRNAs. This would be consistent with prior studies of *Dbp2* and the *GAL* cluster lncRNAs (Cloutier *et al.* 2013). We did not observe antisense transcripts at the ribosome biogenesis snoRNA or mitochondrial respiratory genes, suggesting that this is specific for the *HXT* antisense transcripts.

Loss of *DBP2* affects both sense and antisense hexose transporter transcript levels

The vast majority of antisense transcriptional events correlate with decreased expression of overlapping, protein-coding genes. To determine if there is a general trend between the misregulated antisense transcripts and their corresponding sense targets in *dbp2Δ* cells, we manually selected all transcript pairs whose sense or antisense transcript was differentially expressed with respect to wild type (log₂-fold change greater or less than ±0.5). We then generated a scatter plot of the change in abundance of antisense vs. the sense transcripts for all misregulated genes in *dbp2Δ* cells (Figure 4, gray dots). This revealed no correlation between the upregulated antisense transcripts in *dbp2Δ* cells and the level of the corresponding sense RNA, suggesting that the absence of *DBP2* does not result in a general, genome-wide downregulation of antisense-targeted genes.

Budding yeast encode 17 *HXT* genes whose expression and function constitute the rate-limiting step for glycolysis (Horak 2013). Given the striking enrichment in antisense hexose transporter transcripts in *dbp2Δ* cells (Table 5), we then asked if there was a correlation between sense and antisense *HXT* transcript levels. This revealed a slight positive correlation

between the levels of sense and antisense transcripts corresponding to the *HXT* protein-coding gene products (Figure 4, red dots). In fact, 50% of the *HXT* genes displayed higher sense and antisense *HXT* transcript levels in *dbp2Δ* cells as evidenced by localization in the top, rightmost quadrant. This could occur by simultaneous expression of both, overlapping transcripts in a given cell or by mutually exclusive expression of individual RNAs in different cells within a population. Regardless, this suggests that *Dbp2* regulates the levels of both sense and antisense *HXT* transcripts.

Strand-specific reverse transcriptase-quantitative PCR provides independent validation of differentially expressed *HXT* genes in *dbp2Δ* cells

To independently verify that both sense and antisense *HXT* transcripts are overabundant in *dbp2Δ* cells, we first modified a standard reverse transcriptase-quantitative PCR (RT-qPCR) method to quantify cellular RNAs transcribed from overlapping gene products (Figure 5A). This was necessary as analysis of overlapping transcriptional products is not always straightforward due to vastly different expression levels and the second-strand synthesis activity of reverse transcriptase (Perocchi *et al.* 2007). Strand-specific complementary (c) DNAs were generated using reverse transcription with gene-specific primers (GSPs) to the targeted sequence of interest, and to actin mRNA (*ACT1*) as an internal control, in the presence of actinomycin D (ActD) (Figure 5A). ActD efficiently inhibits second-strand synthesis by reverse transcriptase (data not shown), which has been noted to cause an overrepresentation of antisense transcripts in genome-wide transcriptional studies (Johnson *et al.* 2005; Perocchi *et al.* 2007). Unincorporated GSPs were then removed from the cDNA preparation by standard column chromatography. We selected the *GAL10* sense and antisense RNAs for method validation because the sense and antisense products can be

Table 4 Downregulated Sense Transcripts (700)

| <i>N</i> | LOD | <i>P</i> | <i>P</i> _{adj} | attrib ID | attrib name |
|----------|-------------|----------|-------------------------|------------|---|
| 5 | 1.84052114 | 1.93E-06 | 0.026 | GO:0004169 | Dolichyl-phosphate-mannose-protein mannosyltransferase activity |
| 18 | 0.711054338 | 1.45E-06 | 0.02 | GO:0030561 | RNA 2'-O-ribose methylation guide activity |
| 18 | 0.711054338 | 1.45E-06 | 0.02 | GO:0030562 | rRNA 2'-O-ribose methylation guide activity |
| 20 | 0.693317905 | 6.13E-07 | 0.006 | GO:0031167 | rRNA methylation |
| 21 | 0.685997034 | 3.97E-07 | 0.005 | GO:0031428 | Box C/D snoRNP complex |
| 29 | 0.673647597 | 4.46E-09 | 0 | GO:0000944 | Base pairing with rRNA |
| 28 | 0.667960766 | 1.00E-08 | 0 | GO:0030555 | RNA modification guide activity |
| 28 | 0.667960766 | 1.00E-08 | 0 | GO:0030556 | rRNA modification guide activity |
| 31 | 0.606510897 | 2.03E-08 | 0 | GO:0000154 | rRNA modification |
| 40 | 0.563435455 | 1.89E-09 | 0 | GO:0000496 | Base pairing |
| 39 | 0.551890352 | 5.25E-09 | 0 | GO:0000498 | Base pairing with RNA |
| 39 | 0.535516237 | 1.17E-08 | 0 | GO:0019843 | rRNA binding |
| 34 | 0.530391432 | 1.18E-07 | 0.002 | GO:0005732 | Small nucleolar ribonucleoprotein complex |
| 58 | 0.364279682 | 3.87E-07 | 0.005 | GO:0006520 | Cellular amino acid metabolic process |
| 60 | 0.351442841 | 5.69E-07 | 0.006 | GO:0044106 | Cellular amine metabolic process |
| 62 | 0.346800579 | 4.52E-07 | 0.006 | GO:0006412 | Translation |
| 63 | 0.321570613 | 2.12E-06 | 0.028 | GO:0009308 | Amine metabolic process |
| 77 | 0.313115978 | 3.93E-07 | 0.005 | GO:0044283 | Small molecule biosynthetic process |

Transcripts linked to ribosome biosynthesis, primarily corresponding to small nucleolar RNAs, are downregulated in *dbp2Δ* cells. Genes with sense transcripts that were significantly underrepresented in *dbp2Δ* cells as compared to wild type were selected from the RNA sequencing data set. GO term analysis was conducted using FuncAssociate 2.0 as above. The columns are as follows: **N**, no. of entries in the category; **LOD**, Log10 of the odds ratio; **P**, one-sided *P*-value of the association of attribute and query; **P_{adj}**, adjusted *P*-value as a fraction of 1000 null-hypothesis simulations; **attrib ID**, GO term 8 identification number for attribution category; **attrib name**, category name for functional processes. There was no enrichment of GO terms for downregulated antisense transcripts in *DBP2*-deficient cells.

toggled by growth condition (Houseley *et al.* 2008; Pinskaya *et al.* 2009; Geisler *et al.* 2012). Measurement of *GAL10* transcripts revealed robust expression of sense mRNA above antisense levels in galactose-grown cells and the converse expression pattern in the presence of glucose, consistent with prior studies (Houseley *et al.* 2008; Pinskaya *et al.* 2009; Geisler *et al.* 2012; Figure 5B).

We then utilized strand-specific RT-qPCR to measure the levels of sense and antisense transcripts from four candidate *HXT* genes, *HXT1*, *HXT4*, *HXT5*, and *HXT8*. This revealed over-accumulation of sense transcripts of all four *HXT* genes in *dbp2Δ* cells, with levels ranging from 7- to 17-fold higher than wild type (Figure 5C). *HXT5* exhibits the largest increase, most likely because this moderate affinity hexose transporter is also induced by slow growth rate (Verwaal *et al.* 2002), which is a phenotype of *dbp2Δ* cells (Cloutier *et al.* 2012). Antisense *HXT1*, *HXT5*, and *HXT8* transcripts also accumulate in *dbp2Δ* cells but to a lesser extent than sense gene products (Figure 5D). In contrast, we were unable to detect *HXT4* antisense transcripts in *dbp2Δ* cells (Figure 5D, N.D.), suggesting that some *HXT* antisense lncRNAs are downregulated in the absence of *DBP2*. These measurements by strand-specific RT-qPCR are in line with RNA sequencing quantification, as evidenced by comparison to the RPKM values from wild-type and *dbp2Δ* cells for each *HXT* transcript (Table S2 and Table S3). The absolute fold change in expression between wild-type and *dbp2Δ* cells, however, is different between the two techniques. This is most likely due to normalization differences between these methods; *i.e.*, RT-qPCR is normalized to *ACT1* levels whereas RPKMs are normalized across the length of a transcribed unit. Regardless, this shows that loss of *DBP2* results in simultaneous accumulation of both sense and antisense *HXT* transcripts within a population of cells.

To determine if *Dbp2* plays a direct role in regulation of hexose transporter expression, we then utilized ChIP to ask if *Dbp2* is associated with the genomic regions corresponding to sense and antisense *HXT* transcripts (Figure 5, E and F). ChIP was conducted using a genomically encoded, 3X-FLAG-tagged *DBP2* strain and primer sets corresponding to 5' ends of the *HXT* transcription units, based on the characterized occupancy of *Dbp2* at other genomic loci (Table 2 and Cloutier *et al.* 2012). This revealed that *Dbp2* is associated with chromatin encoding the sense and antisense *HXT1*, *HXT5*, and *HXT8* transcripts (Figure 5, E and F, respectively). *Dbp2* also associates with the 5' end of the *HXT4* sense-coding region (Figure 5E); however, we were unable to test the 5' side of the *HXT4* antisense region due to the lack of unique primer sets for qPCR (Figure 5F). Because each of these genes exhibited aberrant transcript accumulation in *DBP2*-deficient cells, this suggests that *Dbp2* plays a direct role at the *HXT* genes.

Misregulated *HXT* transcripts in *DBP2*-deficient cells are products of normal gene expression

To determine if the expressed *HXT* sense and antisense transcripts in *DBP2*-deficient cells map to the same genomic location as wild-type cells, we utilized the University of California—Santa Cruz (UCSC) genome browser (<http://genome.ucsc.edu/>) to generate representative mapped reads of the *HXT* transcriptional products for both strains (Figure 6, A and B). Consistent with expression of the *HXT* genes, sense-oriented reads fully mapped to the annotated protein coding genes for *HXT1*, *HXT4*, and *HXT5* (Figure 6A). In contrast, however, *HXT8* sequences aligned to an ~1.5-kb region originating within the 3' end of the *HXT8* ORF in both wild-type and *dbp2Δ* cells (Figure 6A, bottom). Interestingly, this transcript

Table 5 Upregulated Antisense Transcripts (382)

| <i>N</i> | LOD | <i>P</i> | <i>P</i> _{adj} | attrib ID | attrib name |
|----------|-------------|----------|-------------------------|------------|--|
| 9 | 1.570899749 | 7.66E-10 | 0 | GO:0005353 | Fructose transmembrane transporter activity |
| 9 | 1.570899749 | 7.66E-10 | 0 | GO:0015578 | Mannose transmembrane transporter activity |
| 9 | 1.508665946 | 1.69E-09 | 0 | GO:0005355 | Glucose transmembrane transporter activity |
| 9 | 1.454222369 | 3.47E-09 | 0 | GO:0015145 | Monosaccharide transmembrane transporter activity |
| 9 | 1.454222369 | 3.47E-09 | 0 | GO:0015149 | Hexose transmembrane transporter activity |
| 11 | 1.340249894 | 4.22E-10 | 0 | GO:0051119 | Sugar transmembrane transporter activity |
| 10 | 1.298536807 | 5.17E-09 | 0 | GO:0008645 | Hexose transport |
| 10 | 1.298536807 | 5.17E-09 | 0 | GO:0015749 | Monosaccharide transport |
| 11 | 1.180032699 | 7.49E-09 | 0 | GO:0015144 | Carbohydrate transmembrane transporter activity |
| 13 | 1.031860845 | 9.38E-09 | 0 | GO:0008643 | Carbohydrate transport |
| 36 | 0.41867088 | 3.33E-06 | 0.047 | GO:0022891 | Substrate-specific <i>trans</i> -membrane transporter activity |

GO term enrichment reveals an overrepresentation of antisense hexose transporter transcripts in *DBP2*-deficient cells. Genes with overlapping, antisense transcripts that were significantly overrepresented in *dbp2Δ* cells as compared to wild type were selected from the RNA sequencing data set. GO term analysis was conducted using FuncAssociate 2.0 as above. The columns are as follows: **N**, no. of entries in the category; **LOD**, Log₁₀ of the odds ratio; **P**, one-sided *P*-value of the association of attribute and query; **P_{adj}**, adjusted *P*-value as a fraction of 1000 null-hypothesis simulations; **attrib ID**, GO term 8 identification number for attribution category; **attrib name**, category name for functional processes.

was also identified in another genome-wide study, indicating that budding yeast predominantly express this 1.5-kb intergenic product instead of *HXT8* ORF mRNAs (Xu *et al.* 2009). Because this study demonstrated accumulation of this transcript under a variety of conditions (varying carbon sources, haploid, diploid), it is currently unknown what, or if any, conditions result in accumulation of a full-length *HXT8* gene product.

Representative reads were also mapped for antisense transcripts corresponding to *HXT1*, 5 and 8 genes in wild-type and *dbp2Δ* cells (Figure 6B). Importantly, the antisense products of *HXT1* and *HXT5* map to the same location as antisense transcripts identified in prior genome-wide transcriptional profiling of wild-type and RNA decay-deficient strains (Xu *et al.* 2009; Van Dijk *et al.* 2011). This suggests that loss of *dbp2Δ* results in upregulation of antisense *HXT1* and *HXT5* gene products that are normally expressed at lower levels in wild-type cells. Antisense *HXT8* transcripts are also present in wild-type cells, albeit at very low levels. Antisense *HXT8* transcription may arise from RNA synthesis within the *HXT8* gene locus or from alternative, upstream initiation of the *YJL215C* locus as noted in prior studies (Xu *et al.* 2009). Regardless, this suggests that antisense transcription is prevalent at *HXT* gene loci and that both sense and antisense transcripts accumulate in *dbp2Δ* cells.

Sense and antisense *HXT* transcripts accumulate in wild-type cells upon glucose deprivation

Given that *Dbp2* is rapidly depleted from the nucleus upon glucose deprivation and that loss of *DBP2* correlates with altered expression of metabolic genes, we asked if regulation of *Dbp2* localization could be an unrecognized mechanism to control gene expression. If this is the case, we proposed that wild-type cells would show a similar expression pattern of *HXT* transcripts as *dbp2Δ* cells when depleted of glucose. To test this, we grew wild-type cells in rich media with glucose (2%) and then subjected the cells to glucose deprivation for 10 min to induce nuclear loss of *Dbp2* (see Figure 1). We then conducted strand-specific RT-qPCR to measure the levels of

sense and antisense *HXT* transcripts (Figure 7, A and B, respectively). Interestingly, this revealed a robust accumulation of *HXT4* and *HXT5* sense transcripts upon glucose deprivation (Figure 7A), reaching levels much higher than those seen in glucose-grown *dbp2Δ* cells (Figure 5, C and D). This difference in expression levels is most likely due to the activity of other nutrient responsive pathways, such as AMPK and PKA/Ras, in addition to *Dbp2*-dependent regulation (Broach 2012). *HXT8* sense transcripts, however, accumulated to similar levels upon glucose deprivation in wild-type cells or deletion of *DBP2*, with a four- to sevenfold increase

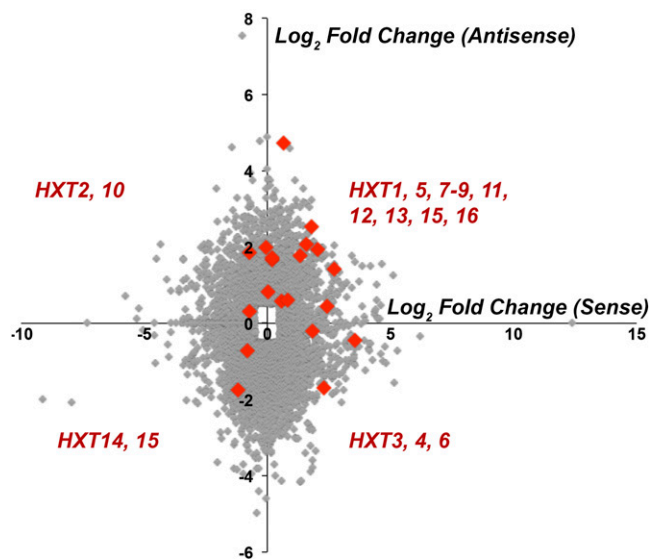


Figure 4 Loss of *DBP2* results in enrichment of sense and antisense hexose transporter gene transcripts. A scatter plot was generated to determine the correlation of sense and antisense transcript pair enrichment in *DBP2*-deficient cells over wild type. Log₂-fold change of transcript abundance is shown for sense transcripts vs. antisense transcripts with substantially increased or decreased transcript levels. Genes that had either sense or antisense transcript reads that were >Log₂ 0.5 or <−0.5 as compared to wild type were selected. Sense and antisense hexose transporter transcript genes (*HXTs*) are shown in red.

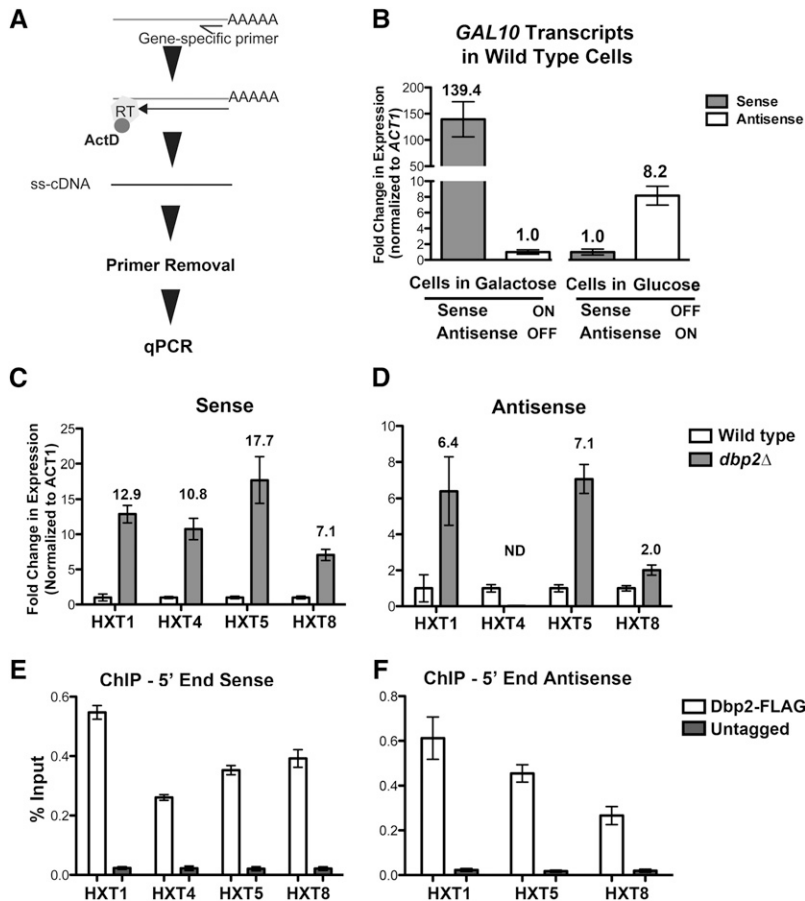


Figure 5 Strand-specific RT-qPCR confirms aberrant *HXT* transcript accumulation in *dbp2Δ* cells, correlating with presence of Dbp2 at genomic *HXT* loci. (A) Stepwise diagram of the strand-specific RT-qPCR method. Reverse transcription is conducted with a gene-specific primer that is complementary to either the sense or antisense strand. Single-stranded cDNA is produced using reverse transcriptase in the presence of actinomycin D (ActD), the latter of which prevents second-strand synthesis (Perocchi *et al.* 2007). Half arrow denotes primer positioning on targeted RNAs whereas complete arrow indicates reverse transcriptase activity. Unincorporated primers are removed using column chromatography and the resulting cDNA is quantified using PCR and SYBR green detection. (B) Single-stranded RT-qPCR measures expression of mutually exclusive *GAL10* sense and antisense transcripts. Total RNA was isolated from wild-type cells grown in triplicate in either glucose or galactose media (for expression of antisense or sense *GAL10* transcripts, respectively) and subjected to transcript-specific cDNA preparation. Gene-specific primers for *ACT1* were also included in the reverse transcription reaction as an internal control for downstream quantification. Fold change in expression was calculated for each growth condition independently and is shown relative to the minority transcript (*i.e.*, transcripts from cells grown in galactose are normalized to antisense *GAL10* and to sense *GAL10* for glucose-cultured cells), which is set to 1 for representation. Numbers above each bar show the average fold change with error bars reflecting the SEM. (C and D) Independent validation of *HXT* sense and antisense transcript abundance using strand-specific RT-qPCR. The fold enrichment of representative *HXT* sense and antisense transcripts in *dbp2Δ* cells over wild type was determined using strand-specific RT-qPCR

as above. Transcript abundance was normalized with respect to *ACT1* transcript levels, a transcript whose levels do not vary between wild-type and *dbp2Δ* cells (Cloutier *et al.* 2012), and is the average of three independent biological replicates and the SEM. ND, not detectible. (E) Dbp2 interacts directly with 5' region of *HXT* genes, with respect to the sense transcript. Chromatin immunoprecipitation of 3X-FLAG-tagged Dbp2 vs. and untagged control strain. Primer-probe sets (Table 2) were designed for sites on genomic DNA corresponding to the 5' regions of the sense transcripts of *HXT1*, *HXT4*, *HXT5*, *HXT8*. (F) Dbp2 interacts directly with the genomic region encoding *HXT* antisense transcripts. Chromatin immunoprecipitation of 3X-FLAG-tagged Dbp2 vs. and untagged control strain. Primer-probe sets (Table 2) were designed for sites on genomic DNA corresponding to the 5' regions of the antisense transcripts of *HXT1*, *HXT5*, *HXT8*. Results are presented as percentage input and are the average of three biological replicates with three technical replicates and the SEM.

in transcript abundance as compared to the control strain (Figure 5 and 7). Antisense *HXT8* transcripts also accumulated in wild-type cells upon glucose depletion (Figure 7B), suggesting that *HXT8* gene expression may be most responsive to glucose-dependent changes in Dbp2 localization. In contrast, we did not observe induction of either sense or antisense *HXT1* transcripts under these conditions, suggesting that altered *HXT1* expression in *dbp2Δ* cells is due to a different mechanism or that Dbp2 may not be fully lost from the *HXT1* locus upon glucose deprivation (Figure 7, A and B). Regardless, loss of *DBP2*, either by genomic mutation or by glucose deprivation, alters the cellular abundance of transcripts corresponding to *HXT* gene loci. Taken together, we suggest that cellular energy homeostasis is dependent on regulation of the RNA helicase Dbp2 and resulting changes in metabolic gene expression.

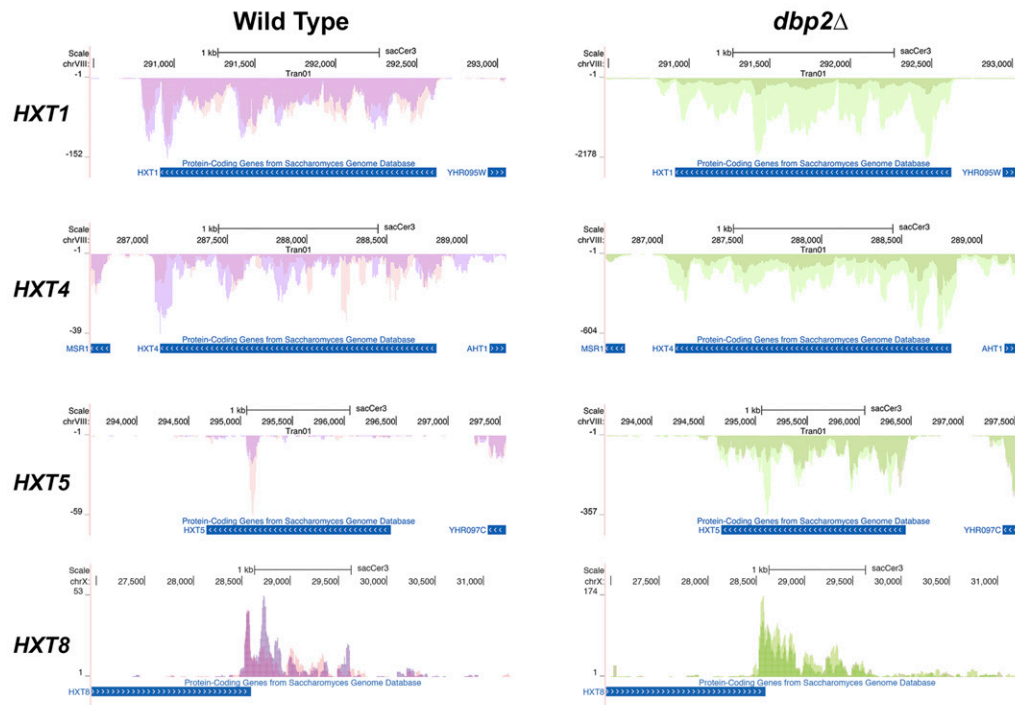
Discussion

Cellular life requires a fine balance between energy generation and consumption to maximize the potential for growth. The

ability to drastically alter the metabolic state of the cell is a hallmark feature of tumor cells called the *Warburg effect*, as well as exercising muscle cells, red blood cells, and activated macrophages and stem cells (Ochocki and Simon 2013; Palsson-Mcdermott and O'Neill 2013). Thus, defining the mechanism(s) governing metabolic control has widespread implications in normal mammalian cell growth and human disease states.

Our results demonstrate that the RNA helicase Dbp2 is a key integrator of nutritional status and gene expression programs required for energy homeostasis. Dbp2 is a canonical member of the DEAD-box family of RNA helicases. Prior work from our laboratory has established that Dbp2 is an RNA-dependent ATPase *in vitro* capable of unwinding a variety of RNA duplex substrates (Cloutier *et al.* 2012; Ma *et al.* 2013). Dbp2 appears to function in multiple aspects of RNA biology including ribosome biogenesis, mRNP assembly, and transcription initiation (Barta and Iggo 1995; Bond *et al.* 2001; Cloutier *et al.* 2012; Ma *et al.* 2013), suggestive of a general role in RNA structure modulation.

A Sense Reads



B Antisense Reads

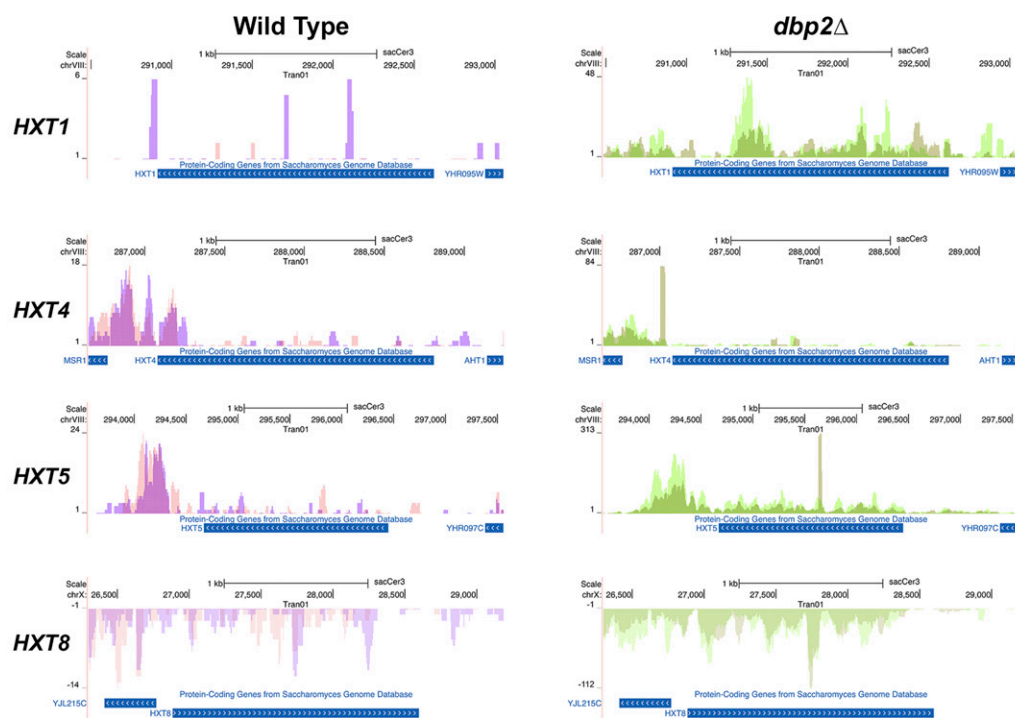


Figure 6 Mapped RNA seq reads across representative HXT genes. Alignment of mapped RNA sequencing reads shows similar (A) sense and (B) antisense expression patterns in wild-type and *dbp2Δ* cells. Reads were aligned to the *S. cerevisiae* genome using the UCSC genome browser. Images were generated directly through the UCSC website and show reads that correspond to the annotated, protein-coding gene. Reads on the top correspond to Watson strand-encoded transcript whereas reads on the bottom of each graph align to a gene encoded on the Crick strand. Arrows within the gene ORF rectangle indicate orientation of the sense transcript within the genome. Sense and antisense transcripts are displayed on different graphs due to differences in abundance and resulting graphical scaling. Note that the y-axis is different between wild-type and *dbp2Δ* cells due to expression level differences between these two strains.

Dbp2 has also been shown to associate with chromatin actively transcribed by RNA polymerase II, indicative of a cotranscriptional role. This is supported by the fact that loss of *DBP2* results in reduced association of mRNA binding proteins and inefficient transcription termination (Cloutier *et al.* 2012; Ma *et al.* 2013). Thus, our work suggests that RNA structure

and/or composition may be central to the metabolic state of the cell.

The ability to match nutrient availability to cellular growth is largely accomplished through the glucose-sensing *Rgt1*–*Snf3*, the TOR, and the AMP-dependent protein kinase (*Snf1* in budding yeast) pathways (Woods *et al.* 1994; Broach

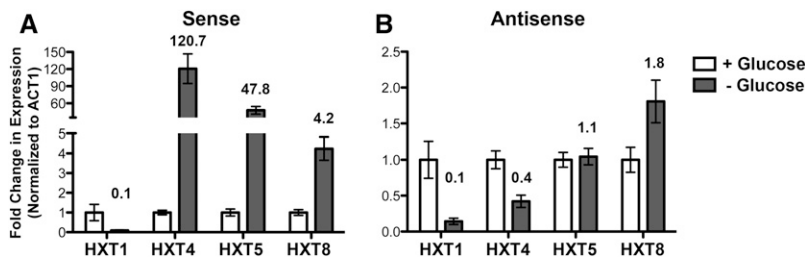


Figure 7 Glucose deprivation alters the levels of sense and antisense hexose transporter transcripts in wild-type cells. HXT sense and antisense transcript abundance using strand-specific RT-qPCR in wild-type cells grown in glucose or after glucose depletion. Wild-type cells were isolated following growth in glucose (2%) or after a 10-min shift to glucose-depleted media. The levels of (A) sense and (B) antisense hexose transporter transcripts were determined by strand-specific RT-qPCR as in Figure 4 and are reported as the average of three biological replicates with the SEM.

2012; Hardie *et al.* 2012; Horak 2013). These signaling programs communicate the presence and concentration of glucose to the energy producing metabolic gene networks and energy-consuming ribosome biogenesis and translational processes. *Snf1* and TOR play opposing roles in cellular homeostasis, with the former increasing energy availability when nutrients are limiting and the latter promoting biogenesis when nutrients are abundant. *Snf1*-dependent relocalization of *Dbp2* to the cytoplasm would be reminiscent of regulated transport of the glucose-dependent repressor *Mig1* whereas TOR signaling would be required to maintain the nuclear pool of *Dbp2* in the presence of glucose. The latter would be similar to glucose-dependent regulation of the transcription factor *Sfp1*, whose nuclear localization is dependent on active TOR and Ras/PKA pathways (Jorgensen *et al.* 2004). However, our results suggest that neither *Snf1* nor TOR signaling play major roles in regulation of *Dbp2* localization in response to glucose availability.

Another possibility is that *Dbp2* directly senses AMP/ATP ratios in the cell. Accumulation of AMP correlates with a decrease in the cellular energy status and occurs upon decreased glucose availability (Boer *et al.* 2010). The AMP-activated protein kinase AMPK is the major energy sensor in eukaryotic cells and is directly regulated by increasing AMP concentrations (Wilson *et al.* 1996; Hardie *et al.* 2012). Interestingly, recent work from the Jankowsky laboratory shows that several DEAD-box RNA helicases are enzymatically inhibited by AMP binding *in vitro*, even though AMP is not a product of ATP hydrolysis (Putnam and Jankowsky 2013a). This included *Mss116* and *Ded1*, which exhibit similar RNA duplex unwinding activities to *Dbp2* (Yang and Jankowsky 2005; Yang *et al.* 2007; Ma *et al.* 2013). Thus, it is tempting to speculate that cellular AMP may directly regulate the helicase activity of *Dbp2*. This is an intriguing possibility, as *Snf1*, the AMPK ortholog in budding yeast, does not directly sense AMP/ATP ratios but is, instead, activated by phosphorylation (Wilson *et al.* 1996; Hardie *et al.* 2012). Further work is necessary to determine if *Dbp2* can act as an AMP sensor to maintain cellular energy homeostasis.

It is currently unknown how *Dbp2* affects cellular RNA levels. Interestingly, rapid changes in carbon sources cause drastic changes in mRNP stability, with ribosomal protein mRNAs undergoing rapid decay upon a glucose to galactose media switch (Munchel *et al.* 2011). It is possible that loss of *Dbp2* results in widespread changes in mRNP/lncRNP composition that alter RNA stability. If this were the case, we would

speculate that these compositional changes occur in the nucleus due to the direct association of *Dbp2* with chromatin (Cloutier *et al.* 2012). Moreover, the similarity between misregulated antisense transcripts in *dbp2Δ* cells and glucose-deprived wild-type cells, when *Dbp2* is cytoplasmic, is consistent with loss of a nuclear role.

In addition to well-known pathways that are glucose dependent, loss of *DBP2* also resulted in upregulation of both sense and antisense *HXT* transcripts. Yeasts in nature encounter a wide range of sugar concentrations that differ by 6 orders of magnitude (from micromolar to molar concentrations) (Johnston and Kim 2005; Horak 2013). A major mechanism to promote growth under these vastly different nutritional conditions is through tight regulation of hexose transporter activity. Although the mechanism(s) that govern transcriptional control of the *HXT* genes are largely established, a role for lncRNAs in this process has not been explored. Previous studies from our laboratory established a role for the *GAL* cluster-associated lncRNAs in facilitating transcriptional switches, enhancing the rate at which the transcriptional activation is stimulated or repressed in response to extracellular cues (Cloutier *et al.* 2013). We would speculate that the antisense *HXT* lncRNAs function similarly, maintaining the activation potential of the *HXT* genes for future restoration of hexose availability. This model is similar to a recently identified Ajar pathway for *HXT5* and recognition of the rapid response rate of yeast upon restoration of nutrients after glucose depletion (Kresnowati *et al.* 2006; Bermejo *et al.* 2010). In fact, upregulation of *HXT5* upon glucose deprivation is specifically required for the rapid restoration of normal growth, suggesting that this pathway allows this single-cell eukaryote to be “optimistic” regarding the return of nutrients in the environment.

An alternative explanation is that the sense and antisense *HXT* transcripts are expressed in different cells within the population, with the antisense transcripts promoting transcriptional repression. If this were the case, the *HXT* lncRNAs may function similarly to *PHO84* lncRNA that functions as a “bimodal” switch to promote different cell fates within a genetically identical population (Castelnuovo *et al.* 2013). A third possibility is that the antisense *HXT* transcripts function in the cytoplasm, controlling translational efficiency to stability of the corresponding sense mRNA (Carrieri *et al.* 2012; Pelechano and Steinmetz 2013; Wang *et al.* 2013). Additional experiments are necessary to uncover potential mechanisms for these antisense lncRNAs in cellular homeostasis. These and future endeavors offer the exciting possibility that lncRNAs, RNA structure,

and/or RNA helicases play specific roles in cellular metabolism.

Acknowledgments

Special thanks go to members of the Tran laboratory for advice and critical reading of this manuscript, to Nadereh Jafari (Northwestern) for assistance with RNA sequencing and bioinformatics, and to Vikki Weake (Purdue) for thoughtful discussion. This work was supported by National Institutes of Health (NIH) R01GM097332-01 to E.J.T.

Literature Cited

- Barta, I., and R. Iggo, 1995 Autoregulation of expression of the yeast Dbp2p 'DEAD-box' protein is mediated by sequences in the conserved DBP2 intron. *EMBO J.* 14: 3800–3808.
- Bermejo, C., F. Haerizadeh, H. Takanaga, D. Chermak, and W. B. Frommer, 2010 Dynamic analysis of cytosolic glucose and ATP levels in yeast using optical sensors. *Biochem. J.* 432: 399–406.
- Berriz, G. F., J. E. Beaver, C. Cenik, M. Tasan, and F. P. Roth, 2009 Next generation software for functional trend analysis. *Bioinformatics* 25: 3043–3044.
- Bhaskaran, H., and R. Russell, 2007 Kinetic redistribution of native and misfolded RNAs by a DEAD-box chaperone. *Nature* 449: 1014–1018.
- Boer, V. M., C. A. Crutchfield, P. H. Bradley, D. Botstein, and J. D. Rabinowitz, 2010 Growth-limiting intracellular metabolites in yeast growing under diverse nutrient limitations. *Mol. Biol. Cell* 21: 198–211.
- Bohnsack, M. T., R. Martin, S. Granneman, M. Ruprecht, E. Schleiff *et al.*, 2009 Prp43 bound at different sites on the pre-rRNA performs distinct functions in ribosome synthesis. *Mol. Cell* 36: 583–592.
- Bond, A. T., D. A. Mangus, F. He, and A. Jacobson, 2001 Absence of Dbp2p alters both nonsense-mediated mRNA decay and rRNA processing. *Mol. Cell. Biol.* 21: 7366–7379.
- Bowers, H. A., P. A. Maroney, M. E. Fairman, B. Kastner, R. Luhrmann *et al.*, 2006 Discriminatory RNP remodeling by the DEAD-box protein DED1. *RNA* 12: 903–912.
- Broach, J. R., 2012 Nutritional control of growth and development in yeast. *Genetics* 192: 73–105.
- Buszczak, M., and A. C. Spradling, 2006 The *Drosophila* P68 RNA helicase regulates transcriptional deactivation by promoting RNA release from chromatin. *Genes Dev.* 20: 977–989.
- Camats, M., S. Guil, M. Kokolo, and M. Bach-Elias, 2008 P68 RNA helicase (DDX5) alters activity of cis- and trans-acting factors of the alternative splicing of H-Ras. *PLoS ONE* 3: e2926.
- Caretti, G., R. L. Schiltz, F. J. Dilworth, M. Di Padova, P. Zhao *et al.*, 2006 The RNA helicases p68/p72 and the noncoding RNA SRA are coregulators of MyoD and skeletal muscle differentiation. *Dev. Cell* 11: 547–560.
- Carrieri, C., L. Cimatti, M. Biagioli, A. Beugnet, S. Zucchelli *et al.*, 2012 Long non-coding antisense RNA controls Uchl1 translation through an embedded SINEB2 repeat. *Nature* 491: 454–457.
- Castelnuovo, M., S. Rahman, E. Guffanti, V. Infantino, F. Stutz *et al.*, 2013 Bimodal expression of PHO84 is modulated by early termination of antisense transcription. *Nat. Struct. Mol. Biol.* 20: 851–858.
- Castoralova, M., D. Brezinova, M. Sveda, J. Lipov, T. Ruml *et al.*, 2012 SUMO-2/3 conjugates accumulating under heat shock or MG132 treatment result largely from new protein synthesis. *Biochim. Biophys. Acta* 1823: 911–919.
- Clark, E. L., A. Coulson, C. Dalglish, P. Rajan, S. M. Nicol *et al.*, 2008 The RNA helicase p68 is a novel androgen receptor co-activator involved in splicing and is overexpressed in prostate cancer. *Cancer Res.* 68: 7938–7946.
- Cloutier, S. C., W. K. Ma, L. T. Nguyen, and E. J. Tran, 2012 The DEAD-box RNA helicase Dbp2 connects RNA quality control with repression of aberrant transcription. *J. Biol. Chem.* 287: 26155–26166.
- Cloutier, S. C., S. Wang, W. K. Ma, C. J. Petell, and E. J. Tran, 2013 Long noncoding RNAs promote transcriptional poisoning of inducible genes. *PLoS Biol.* 11: e1001715.
- Del Campo, M., S. Mohr, Y. Jiang, H. Jia, E. Jankowsky *et al.*, 2009 Unwinding by local strand separation is critical for the function of DEAD-box proteins as RNA chaperones. *J. Mol. Biol.* 389: 674–693.
- De Vit, M. J., J. A. Waddle, and M. Johnston, 1997 Regulated nuclear translocation of the Mig1 glucose repressor. *Mol. Biol. Cell* 8: 1603–1618.
- DeVit, M. J., and M. Johnston, 1999 The nuclear exportin Msn5 is required for nuclear export of the Mig1 glucose repressor of *Saccharomyces cerevisiae*. *Curr. Biol.* 9: 1231–1241.
- Fatica, A., and I. Bozzoni, 2014 Long non-coding RNAs: new players in cell differentiation and development. *Nat. Rev. Genet.* 15: 7–21.
- Fuller-Pace, F. V., and H. C. Moore, 2011 RNA helicases p68 and p72: multifunctional proteins with important implications for cancer development. *Future Oncol.* 7: 239–251.
- Gancedo, J. M., 1998 Yeast carbon catabolite repression. *Microbiol. Mol. Biol. Rev.* 62: 334–361.
- Geisler, S., L. Lojek, A. M. Khalil, K. E. Baker, and J. Collier, 2012 Decapping of long noncoding RNAs regulates inducible genes. *Mol. Cell* 45: 279–291.
- Hardie, D. G., F. A. Ross, and S. A. Hawley, 2012 AMP-activated protein kinase: a target for drugs both ancient and modern. *Chem. Biol.* 19: 1222–1236.
- Horak, J., 2013 Regulations of sugar transporters: insights from yeast. *Curr. Genet.* 59: 1–31.
- Houseley, J., L. Rubbi, M. Grunstein, D. Tollervey, and M. Vogelauer, 2008 A ncRNA modulates histone modification and mRNA induction in the yeast GAL gene cluster. *Mol. Cell* 32: 685–695.
- Jalal, C., H. Uhlmann-Schiffler, and H. Stahl, 2007 Redundant role of DEAD box proteins p68 (Ddx5) and p72/p82 (Ddx17) in ribosome biogenesis and cell proliferation. *Nucleic Acids Res.* 35: 3590–3601.
- Jankowsky, E., 2011 RNA helicases at work: binding and rearranging. *Trends Biochem. Sci.* 36: 19–29.
- Johnson, J. M., S. Edwards, D. Shoemaker, and E. E. Schadt, 2005 Dark matter in the genome: evidence of widespread transcription detected by microarray tiling experiments. *Trends Genet.* 21: 93–102.
- Johnston, M., and J. H. Kim, 2005 Glucose as a hormone: receptor-mediated glucose sensing in the yeast *Saccharomyces cerevisiae*. *Biochem. Soc. Trans.* 33: 247–252.
- Jorgensen, P., I. Rupes, J. R. Sharom, L. Schneper, J. R. Broach *et al.*, 2004 A dynamic transcriptional network communicates growth potential to ribosome synthesis and critical cell size. *Genes Dev.* 18: 2491–2505.
- Kovalev, N., D. Barajas, and P. D. Nagy, 2012 Similar roles for yeast Dbp2 and Arabidopsis RH20 DEAD-box RNA helicases to Ded1 helicase in tombusvirus plus-strand synthesis. *Virology* 432: 470–484.
- Kresnowati, M. T., W. A. van Winden, M. J. Almering, A. ten Pierick, C. Ras *et al.*, 2006 When transcriptome meets metabolome: fast cellular responses of yeast to sudden relief of glucose limitation. *Mol. Syst. Biol.* 2: 49.
- Laxman, S., B. M. Sutter, and B. P. Tu, 2010 Behavior of a metabolic cycling population at the single cell level as visualized by fluorescent gene expression reporters. *PLoS ONE* 5: e12595.
- Lempiainen, H., and D. Shore, 2009 Growth control and ribosome biogenesis. *Curr. Opin. Cell Biol.* 21: 855–863.
- Lohr, D., P. Venkov, and J. Zlatanova, 1995 Transcriptional regulation in the yeast GAL gene family: a complex genetic network. *FASEB J.* 9: 777–787.

- Ma, W. K., S. C. Cloutier, and E. J. Tran, 2013 The DEAD-box protein Dbp2 functions with the RNA-binding protein Yra1 to promote mRNA assembly. *J. Mol. Biol.* 425: 3824–3838.
- Mitchell, S. F., S. Jain, M. She, and R. Parker, 2013 Global analysis of yeast mRNPs. *Nat. Struct. Mol. Biol.* 20: 127–133.
- Munchel, S. E., R. K. Shultzaberger, N. Takizawa, and K. Weis, 2011 Dynamic profiling of mRNA turnover reveals gene-specific and system-wide regulation of mRNA decay. *Mol. Biol. Cell* 22: 2787–2795.
- Ochocki, J. D., and M. C. Simon, 2013 Nutrient-sensing pathways and metabolic regulation in stem cells. *J. Cell Biol.* 203: 23–33.
- Palsson-McDermott, E. M., and L. A. O'Neill, 2013 The Warburg effect then and now: from cancer to inflammatory diseases. *BioEssays* 35: 965–973.
- Pelechano, V., and L. M. Steinmetz, 2013 Gene regulation by antisense transcription. *Nat. Rev. Genet.* 14: 880–893.
- Perocchi, F., Z. Xu, S. Clauder-Munster, and L. M. Steinmetz, 2007 Antisense artifacts in transcriptome microarray experiments are resolved by actinomycin D. *Nucleic Acids Res.* 35: e128.
- Pfaffl, M. W., 2001 A new mathematical model for relative quantification in real-time RT-PCR. *Nucleic Acids Res.* 29: e45.
- Piao, H., J. MacLean Freed, and P. Mayinger, 2012 Metabolic activation of the HOG MAP kinase pathway by Snf1/AMPK regulates lipid signaling at the Golgi. *Traffic* 13: 1522–1531.
- Pinskaya, M., S. Gourvennec, and A. Morillon, 2009 H3 lysine 4-di- and tri-methylation deposited by cryptic transcription attenuates promoter activation. *EMBO J.* 28: 1697–1707.
- Powers, T., and P. Walter, 1999 Regulation of ribosome biogenesis by the rapamycin-sensitive TOR-signaling pathway in *Saccharomyces cerevisiae*. *Mol. Biol. Cell* 10: 987–1000.
- Putnam, A. A., and E. Jankowsky, 2013a AMP sensing by DEAD-box RNA helicases. *J. Mol. Biol.* 425: 3839–3845.
- Putnam, A. A., and E. Jankowsky, 2013b DEAD-box helicases as integrators of RNA, nucleotide and protein binding. *Biochim. Biophys. Acta* 1829: 884–893.
- Ruiz-Echevarria, M. J., C. I. Gonzalez, and S. W. Peltz, 1998 Identifying the right stop: determining how the surveillance complex recognizes and degrades an aberrant mRNA. *EMBO J.* 17: 575–589.
- Salzman, D. W., J. Shubert-Coleman, and H. Furneaux, 2007 P68 RNA helicase unwinds the human let-7 microRNA precursor duplex and is required for let-7-directed silencing of gene expression. *J. Biol. Chem.* 282: 32773–32779.
- Sellick, C. A., R. N. Campbell and R. J. Reece, 2008 Galactose metabolism in yeast-structure and regulation of the leloir pathway enzymes and the genes encoding them. *Int. Rev. Cell Mol. Biol.* 269: 111–150.
- Traven, A., B. Jelcic, and M. Sopta, 2006 Yeast Gal4: a transcriptional paradigm revisited. *EMBO Rep.* 7: 496–499.
- van Dijk, E. L., C. L. Chen, Y. d'Aubenton-Carafa, S. Gourvennec, M. Kwapisz *et al.*, 2011 XUTs are a class of Xrn1-sensitive antisense regulatory non-coding RNA in yeast. *Nature* 475: 114–117.
- Verwaal, R., J. W. Paalman, A. Hogenkamp, A. J. Verkleij, C. T. Verrips *et al.*, 2002 HXT5 expression is determined by growth rates in *Saccharomyces cerevisiae*. *Yeast* 19: 1029–1038.
- Wang, J., C. Gong, and L. E. Maquat, 2013 Control of myogenesis by rodent SINE-containing lncRNAs. *Genes Dev.* 27: 793–804.
- Warner, J. R., 1999 The economics of ribosome biosynthesis in yeast. *Trends Biochem. Sci.* 24: 437–440.
- Westfall, P. J., D. R. Ballon, and J. Thomer, 2004 When the stress of your environment makes you go HOG wild. *Science* 306: 1511–1512.
- Wilson, B. J., G. J. Bates, S. M. Nicol, D. J. Gregory, N. D. Perkins *et al.*, 2004 The p68 and p72 DEAD box RNA helicases interact with HDAC1 and repress transcription in a promoter-specific manner. *BMC Mol. Biol.* 5: 11.
- Wilson, W. A., S. A. Hawley, and D. G. Hardie, 1996 Glucose repression/derepression in budding yeast: SNF1 protein kinase is activated by phosphorylation under derepressing conditions, and this correlates with a high AMP:ATP ratio. *Curr. Biol.* 6: 1426–1434.
- Woods, A., M. R. Munday, J. Scott, X. Yang, M. Carlson *et al.*, 1994 Yeast SNF1 is functionally related to mammalian AMP-activated protein kinase and regulates acetyl-CoA carboxylase in vivo. *J. Biol. Chem.* 269: 19509–19515.
- Wullschlegel, S., R. Loewith, and M. N. Hall, 2006 TOR signaling in growth and metabolism. *Cell* 124: 471–484.
- Xu, Z., W. Wei, J. Gagneur, F. Perocchi, S. Clauder-Munster *et al.*, 2009 Bidirectional promoters generate pervasive transcription in yeast. *Nature* 457: 1033–1037.
- Yang, Q., M. Del Campo, A. M. Lambowitz, and E. Jankowsky, 2007 DEAD-box proteins unwind duplexes by local strand separation. *Mol. Cell* 28: 253–263.
- Yang, Q., and E. Jankowsky, 2005 ATP- and ADP-dependent modulation of RNA unwinding and strand annealing activities by the DEAD-box protein DED1. *Biochemistry* 44: 13591–13601.

Communicating editor: M. Hampsey

GENETICS

Supporting Information

<http://www.genetics.org/lookup/suppl/doi:10.1534/genetics.114.170019/-/DC1>

Regulation of Glucose-Dependent Gene Expression by the RNA Helicase Dbp2 in *Saccharomyces cerevisiae*

Zachary T. Beck, Sara C. Cloutier, Matthew J. Schipma, Christopher J. Petell,
Wai Kit Ma, and Elizabeth J. Tran

Tables S1-S3

Available for download as Excel files at <http://www.genetics.org/lookup/suppl/doi:10.1534/genetics.114.170019/-/DC1>

Table S1 Excel spreadsheet of all annotated *S. cerevisiae* genes with UCSC hyperlinks to the RNA sequencing data set.

Hyperlinks are included that direct to the Saccharomyces Genome Database (yeastgenome.org) or UCSC genome browser (genome.ucsc.org) by clicking on the gene name or the chromosomal location, respectively.

Table S2 Excel spreadsheet of differentially expressed sense transcripts.

The complete list of sense transcripts resulting from RNA sequencing that are differentially expressed (up or down) with respect to wild type following data analysis by Cufflinks 2.0.

Table S3 Excel spreadsheet of differentially expressed antisense transcripts.

The complete list of antisense transcripts resulting from RNA sequencing that are differentially expressed (up or down) with respect to wild type following data analysis by Cufflinks 2.0.